A microscopic model of the dose distribution in hepatocellular carcinoma after selective internal radiation therapy

Elena Cutrì, Ewan Morel–Corlu, Yan Rolland, Hervé Saint-Jalmes, Pierre-Antoine Eliat, Etienne Garin, Johanne Bezy-Wendling

Physica Medica 122 (2024) 103384

Contents lists available at ScienceDirect

Physica Medica

journal homepage: www.elsevier.com/locate/ejmp

A microscopic model of the dose distribution in hepatocellular carcinoma after selective internal radiation therapy

Elena Cutrì [a,b,c,*], Ewan Morel--Corlu [a], Yan Rolland [a], Hervé Saint-Jalmes [a], Pierre-Antoine Eliat [d,e], Etienne Garin [d,f], Johanne Bezy-Wendling [a]

[a] Univ Rennes, CLCC Eugène Marquis, Inserm, LTSI - UMR 1099, F-35000, Rennes, France
[b] Université de technologie de Compiègne, CNRS, Biomechanics and Bioengineering, 60203 Compiègne Cedex, France
[c] Inria, Saclay Ile-de-France, Palaiseau, 91120, France
[d] INRAE, INSERM, Univ Rennes, Nutrition Metabolisms and Cancer, NuMeCan, St Gilles, Rennes, France
[e] CNRS, INSERM, Biosit UAR 3480 US_S 018, PRISM, Univ Rennes, Rennes, France
[f] Department of Nuclear Medicine, Centre Eugène Marquis, Rennes, France

ARTICLE INFO

Keywords:
Hepatocellular carcinoma
Selective internal radiation therapy
Dosimetry evaluation
Microscopic model

ABSTRACT

The dosimetry evaluation for the selective internal radiation therapy is currently performed assuming a uniform activity distribution, which is in contrast with literature findings. A 2D microscopic model of the perfused liver was developed to evaluate the effect of two different ^{90}Y microspheres distributions: i) homogeneous partitioning with the microspheres equally distributed in the perfused liver, and ii) tumor-clustered partitioning where the microspheres distribution is inferred from the patient specific images.

Methods: Two subjects diagnosed with liver cancer were included in this study. For each subject, abdominal CT scans acquired prior to the SIRT and post-treatment ^{90}Y positron emission tomography were considered. Two microspheres partitionings were simulated namely homogeneous and tumor-clustered partitioning. The homogeneous and tumor-clustered partitionings were derived starting from CT images. The microspheres radiation is simulated by means of Russell's law.

Results: In homogenous simulations, the dose delivery is uniform in the whole liver while in the tumor-clustered simulations a heterogeneous distribution of the delivered dose is visible with higher values in the tumor regions. In addition, in the tumor-clustered simulation, the delivered dose is higher in the viable tumor than in the necrotic tumor, for all patients.

In the tumor-clustered case, the dose delivered in the non-tumoral tissue (NTT) was considerably lower than in the perfused liver.

Conclusions: The model proposed here represents a proof-of-concept for personalized dosimetry assessment based on preoperative CT images.

1. Introduction

Selective internal radiation therapy (SIRT) has emerged as an effective treatment for patients suffering from hepatocellular carcinoma (HCC) and liver metastases [1–3]. The treatment consists of intra-arterial administration of radioactive microspheres, typically Yttrium-90 (^{90}Y), via a catheter directly into the hepatic artery [2]. As the blood supply of HCC is mainly provided by the hepatic arterial tree while the portal blood vascularizes the healthy liver parenchyma, the selective radiation of the tumor can be achieved. SIRT can be performed by administering three types of microspheres: ^{90}Y-resin microspheres (SIR-Sphere®, Sirtex Medical Limited Australia, Sydney, Australia), ^{90}Y-glass microspheres (TheraSphere™, Boston Scientific Corporation, Marlborough, MA, USA) and ^{166}Ho-poly-L-lactic acid (PLLA) microspheres (QuiremSpheres®, Quirem Medical B.V., Deventer, The Netherlands). Currently, SIRT is preceded by a pre-treatment assessment, currently called work-up, including a diagnostic liver angiography with intra-arterial injection, at the treatment position, of ^{99m}Tc macro-aggregated albumin (^{99m}Tc-MAA) to perform a liver perfusion scintigraphy using Single Photon Emission Computed Tomography / Computed Tomography ($^{99\,m}$ Tc-MAA SPECT/CT) [4]. For PLLA microspheres, the simulation can also be performed with a scout dose of

* Corresponding author at: Université de Compiègne, CNRS, Biomechanics and Bioengineering, 60203 Compiègne, Cedex.
E-mail address: elena.cutri@utc.fr (E. Cutrì).

https://doi.org/10.1016/j.ejmp.2024.103384
Received 12 October 2023; Received in revised form 3 April 2024; Accepted 21 May 2024
Available online 1 June 2024

PLLA microspheres (Ho-scout) [5]. This work-up is designed to identify the optimal position of the catheter to target the HCC, to ensure no significant extrahepatic radiation (lung and digestive shunts) and to perform dosimetry evaluation. However, a number of uncertainties are associated with this approach which may lead to a sub-optimal outcome of the treatment: the reproducibility of the catheter position during the SIRT, the difference of the particles size and shape between ^{99m}Tc-MAA and the microspheres may lead to a different distribution and dosimetry calculation. Currently there are three SIRT dosimetry models used in the clinical practice, namely the Body Surface Area model (BSA), the Medical Internal Radiation Dose Model (MIRD) and the Partition Model. The BSA model allows the easy calculation of the activity to be administered using only the BSA formula and the tumor burden within the targeted tissue [6,7]. The MIRD model computes the mean absorbed dose in a specific volume of interest (whole liver, lobe, tumor, normal liver) having a given mass and assuming a uniform activity distribution within the target tissue [8,9]. The partition model (PM) also relies on the hypothesis of uniformly distributed activity over a volume, but takes into account for two different regions, namely the tumoral liver and the normal liver. It makes use of the work up assessment as a surrogate of the microsphere's distribution [10,11]. For a more detailed explanation of the dosimetry evaluation for HCC the reader is referred to [12].

For resin microspheres, the most commonly used method is based on the body surface area (BSA), assuming a linear correlation between the liver size and the BSA. Recommendations for glass microspheres given by the TheraSphere Global Dosimetry Steering Committee suggest either the MIRD or the PM dosimetry model for calculating the dose delivery to tumor and normal liver [13,14].

For PLLA microspheres the PM is used based on the PLLA work-up distribution [14–16].

Irrespective of the microsphere's types, all the dosimetry calculations currently performed in the clinical routine assume a uniform activity distribution, disregarding the spatial variation of the dose. Indeed, a great inhomogeneity of ^{90}Y activity in the perfused liver has been reported in literature [17]. This inhomogeneity of the activity is responsible for non-uniform absorbed dose [18,19] and consequently, the radiobiological effects specific to SIRT are poorly estimated.

In addition, there is a large range in the literature regarding dosimetry limits, both for the tumor and the liver [14]. Recent recommendations for resin microspheres suggest that a mean absorbed dose to non-tumoral liver of 40 Gy or less is considered safe (strong agreement) and minimum mean target-absorbed dose to tumor of 100–120 Gy (moderate/strong agreement) [20]. For glass microspheres, Garin and colleagues recently confirmed an improvement in the overall survival in patients if the dose delivered to the tumor is higher than 205 Gy provided that the dose delivery to the non-tumor is lower than 120 Gy [21–24].

In this context, we aim at evaluating the effect of a non-uniform microspheres partitioning on the delivered dose distribution. To this aim, we developed a 2D microscopic model of the perfused liver to reproduce different microspheres distributions in the liver. Firstly, high resolution X-ray-CT imaging on two SIRT-treated livers were used to inform the creation of *in-silico* 2D bounding cases by which ^{90}Y microspheres can be distributed within such organs. Secondly, the radiation dose delivered to regions within the 2D liver slices was assessed for two ^{90}Y microspheres distribution cases: i) homogeneous partitioning with the microspheres equally distributed in the perfused liver, and ii) tumor-clustered partitioning where the microspheres distribution is inferred from the patient specific CT images. The latter partitioning relies on the hypothesis that the microspheres will lodge in the microvasculature visible in the CT scan. Lastly, the computed radiation doses from various zones within these livers were compared to post-treatment ^{90}Y positron emission tomography with integrated computed tomography (^{90}Y PET/CT) spatial imaging of the SIRT-treated livers. ^{90}Y PET/CT allows highly accurate direct imaging of ^{90}Y microspheres distribution and tumor absorbed dose [25,26].

An accurate dosimetry assessment will enable to maximize the local dose delivered to the tumor and to minimize the delivered dose to the nontumoral liver, thus reducing the risk of toxicity. Moreover, by exploiting the capabilities of modern computers, we can envisage the development of personalized dosimetry models.

2. Materials and methods

Two subjects diagnosed with liver cancer were included in this study. The clinical data were collected at the Centre Eugène Marquis (Rennes, France). Both the patients were treated with SIRT with ^{90}Y-glass microspheres (TheraSphere^{TM}) with a microsphere mean diameter of 20 to 30 μm according to manufacturer specifications [27].

One subject (Subject A) is a 50 years old male, without comorbidity, diagnosed in November 2019 with adenocarcinoma in the rectosigmoid junction, and hepatic bilobar metastases. Despite the initial chemotherapy treatment, the hepatic lesions progressed, and a SIRT treatment was planned in November 2020.

The second subject (Subject B) is a 70 years old male, diagnosed with a multifocal hepatocellular carcinoma (HCC) in December 2020, and who underwent a SIRT treatment in June 2021.

2.1. Imaging data

For each subject, abdominal CT scans acquired prior to the SIRT and post-treatment ^{90}Y PET/CT were considered in this study.

Quadriphasic CT scans (SIEMENS SOMATOM Definition AS 64, Siemens Healthineers, Forchheim, Germany) were acquired one week prior to the injection of MAA (single energy CT, 100 kV). First, non-contrast enhanced CT (NC) was acquired followed by the injection of IOMERON 350 contrast agent. For subject A, the arterial phase (AP) scanning was triggered when abdominal aortic density reached 120 HU. The portal-venous phase and delayed phases were acquired after 44 s and after 1 min 42 s, respectively, from the start of injection of intravenous contrast. A different protocol has been used for subject B to collect data for a parallel study. First, a NC CT was acquired, an AP CT was acquired when the aortic grey intensity reached 100 HU, closely followed by another AP CT with a 25 s delay. Finally, a portal venous phase was acquired after 40 s. Any future reference to subject B's AP-CT refers to the second AP-CT performed according to this protocol.

The 4 CT-scan data sets (2 for each subject) comprise slice-wise images (from 221 and 254 slices) with a spatial resolution ranging between 0.71 mm x 0.71 mm and 0.87 mm x 0.87 mm, a slice thickness of 2 mm and a slice spacing of 1 mm.

The 2D AP CT slices used for the two subjects are shown in Fig. 1 (top panel). For the subject A four lesions are visible, with the major lesion located in the hepatic dome (58 mm diameter). Two AP CT slices were considered for subject B: one slice (subject B1) assessed the presence of two hyper arterial lesions, one in the V segment (100 mm diameter), and one in the VIII segment (37 mm diameter) and slice 2 (subject B2) shows only the presence of the lesion in segment V.

^{90}Y PET/CT was performed on PET QC1500 GE medical systems (Chicago, USA).

^{90}Y PET/CT imaging is based on a minor decay branch of ^{90}Y resulting in the generation of annihilation photons. Yttrium-90 decays to the 0 + first excited state of zirconium-90, followed by the emission of an electron–positron internal pair at a very low branching ratio [28].

Despite the low branching fraction for positron emission, it is possible to obtain high-resolution images of microspheres distribution using conventional time-of-flight PET scanners, with only minor adjustments to scan technique and image reconstruction [25].

^{90}Y PET/CT images (Fig. 1, bottom panel) showed activity in both the right and left lobes for subject A while for subject B's there is only activity in the right lobe.

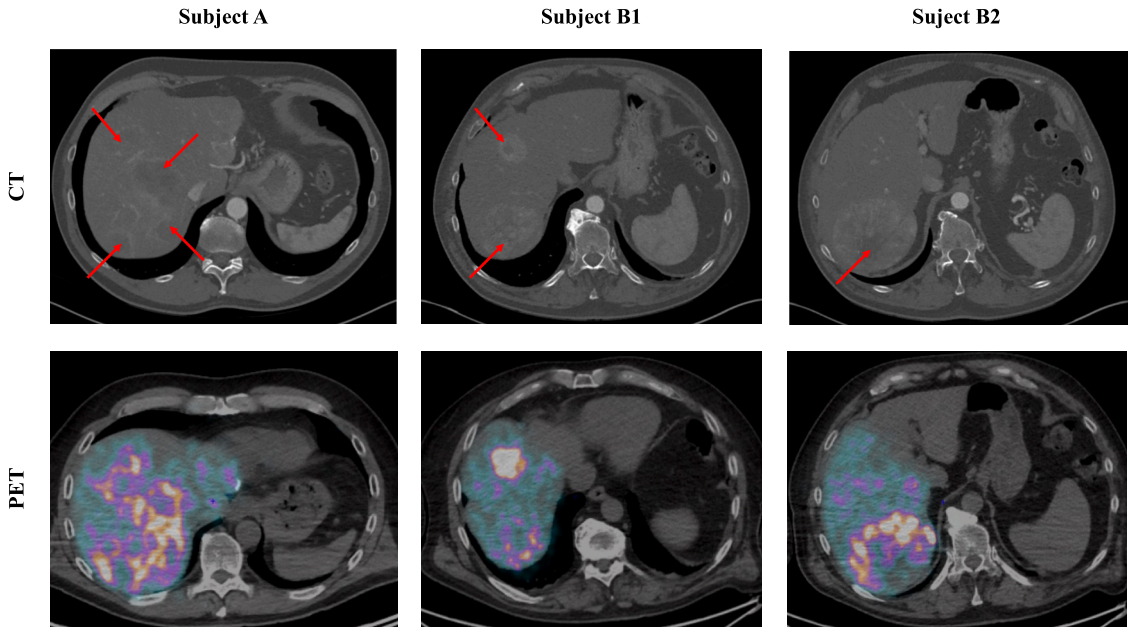

Fig. 1. Top panel: arterial phase CT scan for Subject A (left (A) with four visible lesions (red arrows)), for Subject B1(center) with two visible lesions (red arrows) and subject B2 (right) with only one tumor visible (red arrow). Bottom panel: Post-treatment ^{90}Y PET/CT scan for Subject A (left), Subject B1(center) and Subject B2 (right).

2.2. *Administered TheraSphere™ activity*

The activity to be administered to the subjects has been computed based on the personalized dosimetry approach proposed in [21–24]. The planned activity to be administered to subject A was 3.27 GBq of TheraSphere™ in the right hepatic artery and 0.43 GBq in the left hepatic artery for an expected delivered dose of 86.3 Gy and 81 Gy to the right and left lobe, respectively and 97.6 Gy to the whole liver.

For subject B, the planned activity to administer was of 6.44 GBq in the right hepatic artery for an expected delivered dose of 166 Gy in the right lobe (132.5 Gy to the whole liver), 237 Gy to the large lesion, 398 Gy to the small lesion, and 143 Gy to the healthy treated liver (104 Gy to the whole healthy liver).

2.3. *Microscopic model*

The microscopic model proposed here is based on a simplification of the Functional Sub-Unit (FSU) of the liver, namely the hepatic lobule. Each hepatic lobule is modeled as a hexagonal prism with a height (h) of 1.5 mm as defined by [29]. Each lobule has 6 vertices corresponding to the hepatic triad where the microspheres can be lodged. The hexagonal lobule is then arranged in a lattice representing a part of the liver. By matching the lattice of lobules to the DICOM images, the spatial distribution of the vertices can be derived and the number of vertices per image pixel obtained. Multiplying the latter by the number of microspheres to be placed at that point gives the 2D microspheres partitioning.

2.4. *Microsphere's partitioning*

Two microspheres partitionings were simulated: i) homogeneous with the total of microspheres equally distributed in the perfused liver, and ii) tumor-clustered, with the density of microspheres in the perfused liver inferred from the intensity scale of the native CT images. The

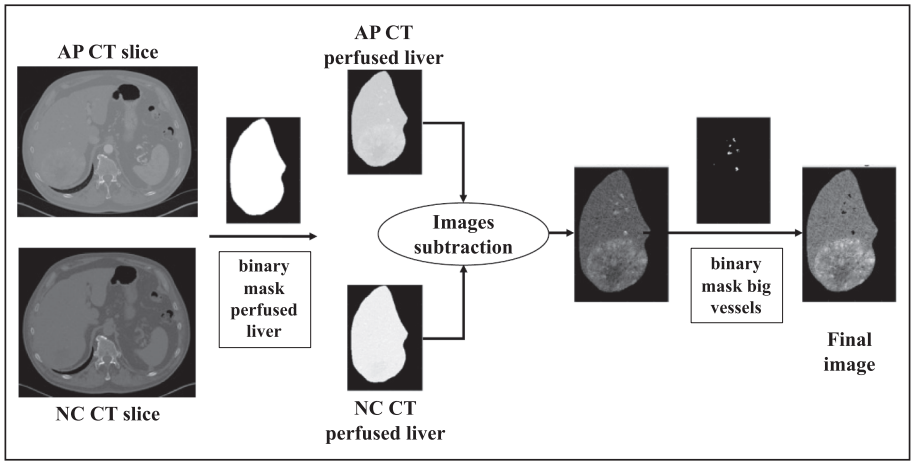

Fig. 2. Methodology to obtain the starting image for the tumor-clustered partitioning. For each subject, the NC CT image sequence and AP CT slices were firstly registered. Secondly, a binary mask was applied to the AP CT and NC CT to identify the perfused liver. Thirdly, an image subtraction was performed to enhance the perfused liver. Lastly, a binary mask was applied to delete the big vessels.

homogeneous and tumor-clustered partitionings were derived starting from CT images. The methodology applied is summarized in Fig. 2. This methodology is based on two main assumptions. Firstly, as the microspheres are transported by arterial blood flow, they will lodge in the hepatic arterial tree and more specifically in vessels of comparable size (of the order of a few tens of micrometers). Secondly, the density of these hepatic arterial vessels can be visualized and quantified by differential CT (notably by subtracting AP CT and NC CT sequences) [30]. For each subject two CT slices were considered, one from the NC CT image sequence and one from the AP CT sequence. The two images were firstly registered using a non-rigid, intensity-based algorithm [31,32]. Secondly, a binary mask was applied to the AP CT and NC CT to identify the liver segments to be targeted with the SIRT (hereinafter referred as perfused liver). Thirdly, an image subtraction step was performed to enhance the perfused liver (image subtraction). Finally, a binary mask identifying large vessels was constructed and applied to remove these vessels from the image, as the microspheres would not fit into them.

From this image, the homogeneous and tumor-clustered partitions are constructed, the former by placing microspheres in correspondence with each vertex of the hepatic lobules in the image, and the latter by deducing the density of microspheres in proportion to image intensity. For each subject, the total number of microspheres considered for the homogeneous and tumor-clustered partitionings was estimated from the density of microspheres per unit volume computed from patient specific MAA SPECT/CT as the ratio of the injected microspheres over the targeted liver volume. The number of microspheres in each vertex can range from 0 (being the lowest grey level) to 6 (being the highest intensity level).

The final microspheres partitionings for the homogeneous and tumor-clustered scenarios, for subject A and B, are illustrated in Fig. 3.

After all the microspheres are placed, the radiation is simulated by means of Russell's law [33]:

$$D = 0.989A\frac{1-\frac{r}{8}}{r^2}$$

where D is the absorbed dose in Gy, A is the activity of the radioactive compound in kBq, and r is the distance to the source in mm. This law allows the calculation of the delivered dose in each point of the model based on the activity of each microsphere and its distance from the considered point. Each microsphere is modelled as a point-like source. The activity for each microsphere was set at 2.5 kBq to simulate the injection of TheraSphere^{TM} microspheres [27]. As ^{90}Y mainly decays via beta emissions, we considered it as a pure beta emitter [34].

3. Results

3.1. Microscopic model validation

To validate the calculation of the delivered dose obtained with microscopic model, we performed two simplified simulations: i) a **2D single lobule simulation** with one Therasphere^{TM} located in each of the hepatic lobule's vertex, ii) a **2D multi-lobular simulation** consisting of 20 by 20 lobules with one Therasphere^{TM} per vertex. The same simulations were performed by using Geant4 Application for Tomographic Emission (GATE) [35], an open-source program used for dosimetry evaluation.

The geometry of the hepatic lobule used in the GATE simulations is shown in Fig. 4 with detailed dimensional information as proposed by [29].

The healthy liver material as well as the not–tumoral tissue (NTT)

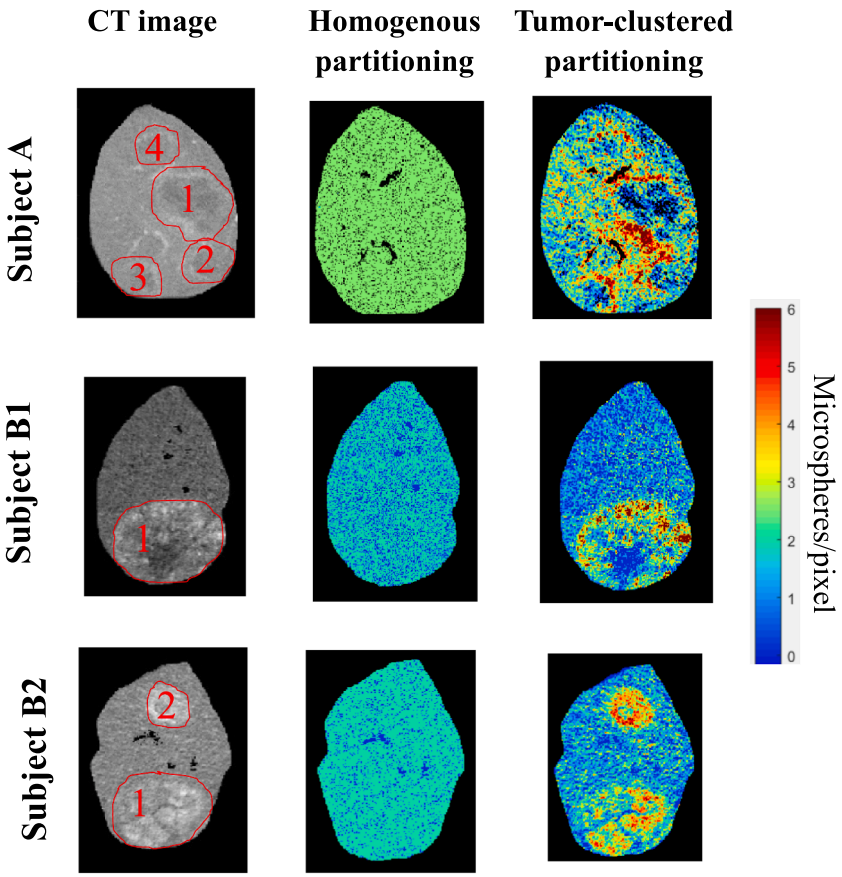

Fig. 3. The CT final image, the partitioning of the microspheres for the homogeneous and tumor-clustered cases are shown for the subject A, B1 and B2; the tumor numbering adopted in this study is reported in the CT final image.

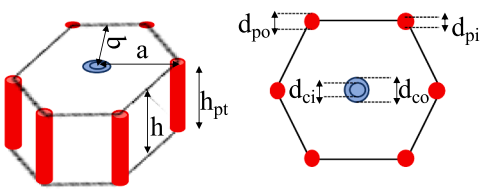

	[μm]		[μm]
h	1500	d_{po}	48
h_{pt}	1300	d_{pi}	30
a	600	d_{co}	66
b	693	d_{ci}	56

Fig. 4. Hepatic lobule geometry. h is the lobule height, h_{pt} is the hepatic artery and central vein heights, a is the lobule radius, b is the distance from centre, d_{po} and d_{pi} are the hepatic arteriole outer and inner diameters, respectively, d_{co} and d_{ci} are the central vein outer and inner diameters, respectively.

were modelled by using the LIVER material already implemented in GATE. To simulate the injection of Therasphere™, different physical processes were considered, namely the Photoelectric effect, the Compton scattering, the Rayleigh scattering, the Pair production effect, the Electron ionization, the Bremsstrahlung, the positron annihilation and the radioactive decay [35].

The activity of the Therasphere™ was set at 2.5 kBq both in the microscopic model and in GATE simulation. The mean delivered dose calculated with the microscopic model was 64 Gy and 81 Gy in the single lobule simulation and in the multi-lobular geometry, respectively, in agreement with the results obtained using GATE.

3.2. Microscopic model results

The simulated dose delivery for the two subjects is shown in Fig. 5 for the homogeneous and tumor-clustered cases. As expected, in the homogeneous simulations, the dose delivery is uniform throughout the liver, whereas in the simulations with tumor clusters, a heterogeneous distribution of the mean dose is visible. In particular, for subject A, in the simulation with tumor clusters, the highest value is found at the periphery of tumor 1, and for subject B, in both slices, the delivered dose is higher in correspondence with the tumors.

For each simulation, the mean delivered dose was computed in the perfused liver, the not tumoral tissue (NTT), i.e., the part of the perfused liver without tumoral lesion and for each individual tumor. In addition, for each tumor, the mean delivered dose was computed in two different

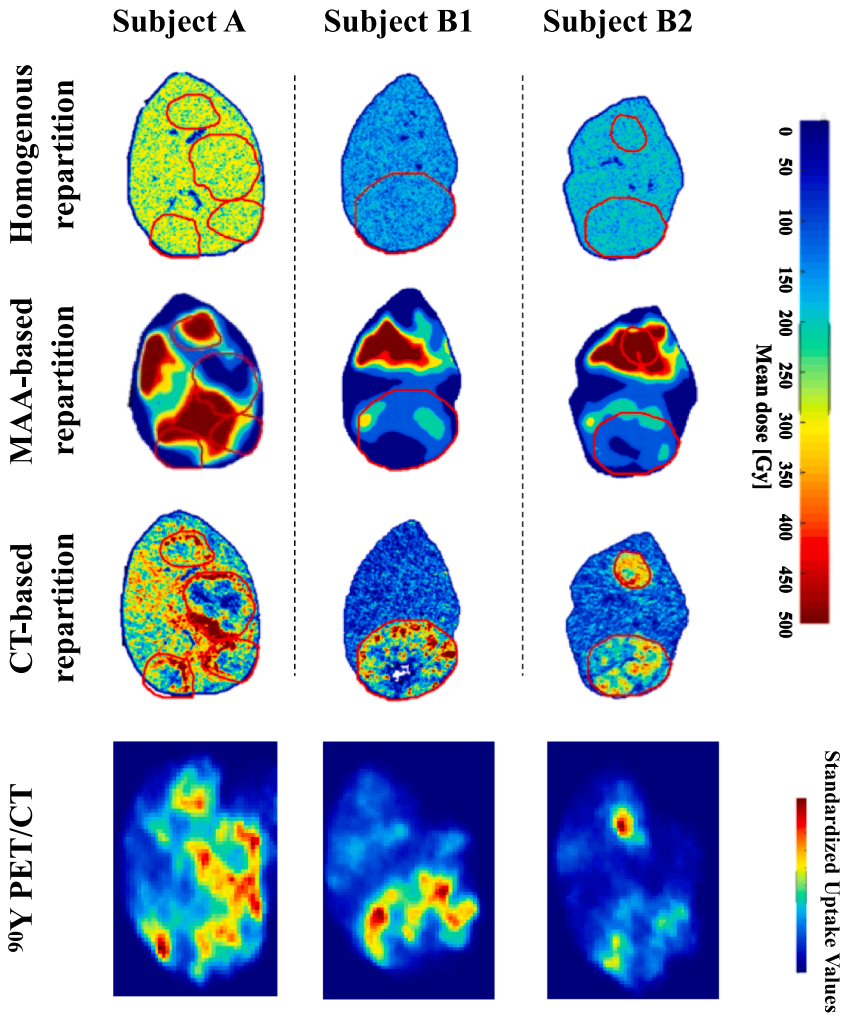

Fig. 5. 2D delivered dose distributions for the homogeneous (1st row) and tumor-clustered (3rd row) simulations subject A, subject B1 and B2. The red circles highlight the tumors. Post-operative ^{90}Y PET/CT slice for subject A, B1 and B2 is shown in the 3rd row.

parts, namely the viable tumor which is the part of the tumor with the vasculature and the necrotic tumor i.e., the dead core (Table 1 for subject A, Table 2 for subject B1 and Table 3 for subject B2). Viable and necrotic parts of the tumor were identified from the CT images, setting a grayscale threshold for both, then manually refining the resulting regions.

For each subject, the mean delivered doses in the whole perfused liver computed for the homogeneous, and tumor-clustered case are similar (max error < 2.7 %), as the number of injected microspheres is the same (subject A: 247 ± 81 Gy for the homogeneous case vs 247 ± 131 Gy for tumor-clustered case; subject B1: 142 ± 52 Gy for the homogeneous case vs 142 ± 113 Gy for tumor-clustered case; subject B2: 169 ± 51 Gy for the homogeneous case vs 169 ± 108 Gy for tumor-clustered case) (Tables 1-3).

For a homogenous partitioning of microspheres, the mean delivered dose for each subject is similar in each considered region (perfused, NTT, whole tumor, viable tumor, necrotic tumor) which is not surprising given that in this model the radiative pseudo-point sources are uniformly distributed throughout the entire perfused liver.

In the tumor-clustered simulation, a higher dose was delivered to the viable tumor vs the necrotic tumor for all the patients (subject A: 363 ± 133 Gy vs 147 ± 89 Gy, 351 ± 134 Gy vs 182 ± 86 Gy, 295 ± 152 Gy vs 167 ± 102 Gy, 317 ± 89 Gy vs 227 ± 74 Gy, respectively in tumor 1, tumor 2, tumor 3 and tumor 4; subject B1: 242 ± 130 Gy vs 66 ± 60 Gy, in tumor 1; subject B2: 266 ± 95 Gy vs 163 ± 71 Gy and 362 ± 85 Gy vs 267 ± 64 Gy, respectively in tumor 1 and tumor 2) (Tables 1-3).

The comparison of the mean delivered dose in the perfused liver vs the NTT in the tumor-clustered case highlighted a dose delivery to the NTT considerably lower than that delivered dose computed in the perfused liver (subject A: 247 ± 131 Gy to the perfused liver vs 231 ± 118 Gy to the NTT; subject B1: 142 ± 113 Gy to the perfused liver vs 94 ± 57 Gy to the NTT; subject B2: 169 ± 108 Gy to the perfused liver vs 121 ± 68 Gy to the NTT) (Tables 1-3).

4. Discussion

The analysis of the dose distribution allows to draw interesting information. Firstly, the assumption of a uniform distribution of microspheres that underlies the methods currently used in clinical practice to assess dosimetry seems unrealistic. Indeed, when comparing the simulated dose distribution in the homogeneous case and corresponding post-operative ^{90}Y PET/CT a strong discrepancy was found for all the subjects. This means that assuming an even distribution of the microspheres in the target region represents a strong approximation and the authors suggest to account for the patient specific vasculature as well as for tumor morphology to provide more accurate dosimetry estimation.

Secondly, an overall good agreement of the dose distribution computed with the tumor-clustered simulation and post-operative ^{90}Y PET/CT of the subject was found. Indeed, for subject A the higher delivery dose found via the simulation and in the post-operative images is located in between tumor 1 and 2 and in tumor 3 (more evident in the ^{90}Y PET/CT). Similarly, the comparison of ^{90}Y PET/CT image and the tumor-clustered simulation results of subject B1 shows a comparable distribution of the delivery dose in the perfused liver, with a peak in correspondence of the tumor 2 (Fig. 5). The same pattern of the delivered dose distribution was also found for the ^{90}Y PET/CT image and the tumor-clustered simulation results for the subject B2 with a more uniform delivered dose distribution in tumor 2 in the case of ^{90}Y PET/CT image (Fig. 5).

Thirdly, the evaluation of the delivered dose to the viable vs the necrotic tumor for the tumor-clustered simulated partitioning showed that the viable lesion received a higher absorbed dose than the necrotic tumor. This finding supports the hypothesis that the microspheres partitioning can be derived from the analysis of patient images.

Lastly, an improvement in the overall survival in patients treated with glass microspheres has been assessed in the literature [19] if the dose delivered to the tumor is higher than 205 Gy, and the dose delivered to the non-tumor is lower than 120 Gy. In our simulation, the dose delivered to the NTT was higher than 120 Gy for all microspheres partitionings for all the subjects (except the tumor-clustered case in subject

Table 1
2D Delivered dose (mean ± SD) obtained by the 2 simulations methods (homogeneous and tumor-clustered) in perfused liver, the NTT, for each tumor, for the viable tumor and the necrotic tumor for Subject A. For the tumor numbering the reader is referred to Fig. 3.

	Homogeneous delivered dose [Gy]	Tumor-clustered delivered dose [Gy]
Perfused liver	247 ± 81	247 ± 131
NTT	234 ± 92	231 ± 118
	Tumor 1	
Whole tumor	274 ± 40	270 ± 158
Viable tumor	275 ± 39	363 ± 133
Necrotic tumor	272 ± 41	147 ± 89
	Tumor 2	
Whole tumor	258 ± 64	271 ± 142
Viable tumor	259 ± 62	351 ± 134
Necrotic tumor	256 ± 67	182 ± 86
	Tumor 3	
Whole tumor	242 ± 86	244 ± 148
Viable tumor	244 ± 87	295 ± 152
Necrotic tumor	240 ± 86	167 ± 102
	Tumor 4	
Whole tumor	271 ± 40	294 ± 94
Viable tumor	271 ± 40	317 ± 89
Necrotic tumor	269 ± 40	227 ± 74

Table 2
2D delivered dose (mean ± SD) obtained by the 2 simulations methods (homogeneous and tumor-clustered) in perfused liver, the NTT, for each tumor, for the viable tumor and the necrotic tumor for Subject B1. For the tumor numbering the reader is referred to Fig. 3.

	Homogeneous delivered dose [Gy]	Tumor-clustered delivered dose [Gy]
Perfused liver	142 ± 52	142 ± 113
NTT	138 ± 55	94 ± 57
	Tumor 1	
Whole tumor	147 ± 48	217 ± 137
Viable tumor	146 ± 48	242 ± 130
Necrotic tumor	152 ± 43	66 ± 60

Table 3
2D delivered dose (mean ± SD) obtained by the 2 simulations methods (homogeneous and tumor-clustered) in perfused liver, the NTT, for each tumor, for the viable tumor and the necrotic tumor for Subject B2. For the tumor numbering the reader is referred to Fig. 3.

	Homogeneous delivered dose [Gy]	Tumor-clustered delivered dose [Gy]
Perfused liver	169 ± 51	169 ± 108
NTT	163 ± 57	121 ± 68
	Tumor 1	
Whole tumor	182 ± 32	245 ± 100
Viable tumor	183 ± 32	266 ± 95
Necrotic tumor	179 ± 32	163 ± 71
	Tumor 2	
Whole tumor	185 ± 28	354 ± 87
Viable tumor	185 ± 29	362 ± 85
Necrotic tumor	180 ± 26	267 ± 64

B1). This suggests that attaining good patient-specific microscopic dose delivery plans will involve careful assessment of locally-delivered doses to both tumoral and NTT regions.

The results of the simulation are affected by the model limitation which are addressed below.

As the total number of microspheres delivered to the simulated liver is not known, this parameter was arbitrarily chosen starting from the MAA SPECT/CT information. This choice represents a strong approximation as the absolute values of dose is highly sensitive to this number of microspheres. However, for a given number of injected microspheres, the comparison of the dose distribution in the homogeneous and tumor-clustered partitionings of the same subject as well as in the tumor vs NTT holds true. To obtain an accurate prediction of the delivered dose distribution, the real number of microspheres injected during the treatment must be used.

In this study, we developed a 2D model to verify if our hypothesis of inferring information of the microsphere's distribution from patient specific CT images was reliable. Even if the results here presented showed a good overall agreement with patient post ^{90}Y PET/CT data, the use of a 3D model will allow to also account for the volumetric contribution of the delivered dose.

The dose delivery to the liver has been modelled using a simple law which provides the spatial distribution of the delivered dose secondary to the presence of a source with a given initial activity. The use of a more sophisticated representation of this phenomenon may provide more accurate results.

The model results have been only qualitatively compared with clinical post-operative data. The use of a 3D model and of real number of microspheres injected into the hepatic tree will allow to quantitatively validate the results against subject specific clinical data.

Lastly, the identification of the tumor burden as well as of the viable and necrotic region of the tumor has been performed by using a thresholding of intensity level on the CT final images. A more accurate identification of such regions by performing a 3D segmentation will provide more realistic results.

5. Conclusion

The objective of this study was to develop a model to predict the delivered dose distribution within the liver tumor by relying on patient specific pre-operative images. A good agreement of the tumor-clustered case simulation with the post-operative ^{90}Y PET/CT was found.

In this respect, the model proposed here represents a proof of concept for personalized dosimetry assessment based on preoperative CT images. In this light, the extension of the model to a 3D representation of the perfused liver will inform the interventional radiologist on the possible microspheres partitioning at a microscopic scale, and consequently on the local dose delivery thus providing important information on the dosimetry evaluation.

Declaration of competing interest

The authors declare that they have no known competing financial interests or personal relationships that could have appeared to influence the work reported in this paper.

Acknowledgments

This study was supported by the 'Innovation collaborative au croisement des filières' grant funded by the region of Brittany and the European Community for the project '*Assistance à la RtMi par un Outil temps Réel en routine clinIQUE - ARMORIQUE*' (2019-2022).

References

[1] Kennedy A, Nag S, Salem R, et al. Recommendations for radioembolization of hepatic malignancies using yttrium-90 microsphere brachytherapy: a consensus panel report from the radioembolization brachytherapy oncology consortium. Int J Radiat Oncol Biol Phys 2007 May 1;68(1):13–23.
[2] Sangro B, Bilbao JI, Boan J, et al. Radioembolization using 90Y-resin microspheres for patients with advanced hepatocellular carcinoma. Int J Radiat Oncol Biol Phys 2006 Nov 1;66(3):792–800.
[3] Saxena A, Bester L, Shan L, et al. A systematic review on the safety and efficacy of yttrium-90 radioembolization for unresectable, chemorefractory colorectal cancer liver metastases. J Cancer Res Clin Oncol 2014 Apr;140(4):537–47.
[4] Garin E, Rolland Y, Laffont S, Edeline J. Clinical impact of (99m) Tc-MAA SPECT/CT-based dosimetry in the radioembolization of liver malignancies with (90)Y-loaded microspheres. Eur J Nucl Med Mol Imag 2016;43:559–75.
[5] Braat AJAT, Prince JF, van Rooij R, Bruijnen RCG, van den Bosch MAAJ, Lam MGEH. Safety analysis of holmium-166 microsphere scout dose imaging during radioembolisation work-up: a cohort study. Eur Radiol 2018;28(3):920–8.
[6] Kao YH, Tan EH, Ng CE, Goh SW. Clinical implications of the body surface area method versus partition model dosimetry for yttrium-90 radioembolization using resin microspheres: a technical review. Ann Nucl Med 2011 Aug;25(7):455–61.
[7] Tong AK, Kao YH, Too CW, Chin KF, Ng DC, Chow PK. Yttrium-90 hepatic radioembolization: clinical review and current techniques in interventional radiology and personalized dosimetry. Br J Radiol 2016 Jun;89(1062):20150943.
[8] Gulec SA, Mesoloras G, Stabin M. Dosimetric techniques in 90Y-microsphere therapy of liver cancer: The MIRD equations for dose calculations. J Nucl Med 2006 Jul;47(7):1209–11. PMID: 16818957.
[9] Dezarn WA, Cessna JT, DeWerd LA, et al. Recommendations of the American Association of Physicists in Medicine on dosimetry, imaging, and quality assurance procedures for 90Y microsphere brachytherapy in the treatment of hepatic malignancies. Med Phys 2011 Aug;38(8):4824–45.
[10] Ho S, Lau WY, Leung TW, et al. Partition model for estimating radiation doses from yttrium-90 microspheres in treating hepatic tumours. Eur J Nucl Med 1996 Aug;23(8):947–52.
[11] Ho S, Lau WY, Leung TW, Chan M, Johnson PJ, Li AK. Clinical evaluation of the partition model for estimating radiation doses from yttrium-90 microspheres in the treatment of hepatic cancer. Eur J Nucl Med 1997 Mar;24(3):293–8.
[12] Gulec SA, McGoron AJ. Radiomicrosphere Dosimetry: Principles and Current State of the Art. Semin Nucl Med 2022 Mar;52(2):215–28.
[13] Saini A, Wallace A, Alzubaidi S, et al. History and Evolution of Yttrium-90 Radioembolization for Hepatocellular Carcinoma. J Clin Med 2019 Jan 7;8(1):55.
[14] Bastiaannet R, Kappadath SC, Kunnen B, Braat AJAT, Lam MGEH, de Jong HWAM. The physics of radioembolization EJNMMI Phys 2018 Nov 2;5(1):22.
[15] Smits ML, Nijsen JF, van den Bosch MA, et al. Holmium-166 radioembolization for the treatment of patients with liver metastases: design of the phase I HEPAR trial. J Exp Clin Cancer Res 2010. Jun 15;29(1):70.
[16] James T, Hill J, Fahrbach T, Collins Z. Differences in Radiation Activity Between Glass and Resin 90Y Microspheres in Treating Unresectable Hepatic Cancer. Health Phys 2017 Mar;112(3):300–4.
[17] Ng SC, Lee VH, Law MW, Liu RK, Ma VW, Tso WK, et al. Patient dosimetry for 90Y selective internal radiation treatment based on 90Y PET imaging. J Appl Clin Med Phys 2013 Sep 6;14(5):212–21.
[18] Högberg J, Rizell M, Hultborn R, et al. Heterogeneity of microsphere distribution in resected liver and tumour tissue following selective intrahepatic radiotherapy. EJNMMI Res 2014 Dec;4(1):48.
[19] Högberg J, Rizell M, Hultborn R, et al. Increased absorbed liver dose in Selective Internal Radiation Therapy (SIRT) correlates with increased sphere-cluster frequency and absorbed dose inhomogeneity. EJNMMI Phys 2015 Dec;2(1):10.
[20] Levillain H, Bagni O, Deroose CM, et al. International recommendations for personalised selective internal radiation therapy of primary and metastatic liver diseases with yttrium-90 resin microspheres. Eur J Nucl Med Mol Imaging 2021 May;48(5):1570–84.
[21] Garin E, Lenoir L, Rolland Y, et al. Dosimetry based on 99mTc-macroaggregated albumin SPECT/CT accurately predicts tumor response and survival in hepatocellular carcinoma patients treated with 90Y-loaded glass microspheres: preliminary results. J Nucl Med 2012 Feb;53(2):255–63.
[22] Eur J Nucl Med MolImag 2013;40:1057–68.
[23] Garin E, Rolland Y, Edeline J, et al. Personalized dosimetry with intensification using 90Y-loaded glass microsphere radioembolization induces prolonged overall survival in hepatocellular carcinoma patients with portal vein thrombosis. J Nucl Med 2015 Mar;56(3):339–46.
[24] Garin E, Tselikas L, Guiu B, et al. Personalised versus standard dosimetry approach of selective internal radiation therapy in patients with locally advanced hepatocellular carcinoma (DOSISPHERE-01): a randomised, multicentre, open-label phase 2 trial. Lancet Gastroenterol Hepatol 2021 Jan;6(1):17–29.
[25] Kao YH, Steinberg JD, Tay YS, Lim GK, Yan J, Townsend DW, et al. Post-radioembolization yttrium-90 PET/CT - part 1: diagnostic reporting. EJNMMI Res 2013 Jul 25;3(1):56.
[26] Tafti BA, Padia SA. Dosimetry of Y-90 Microspheres Utilizing Tc-99m SPECT and Y-90 PET. Semin Nucl Med 2019 May;49(3):211–7.
[27] Therasphere™ Y-90 Glass Microspheres, Dose matters, Boston Scientific, https://www.bostonscientific.com/content/dam/bostonscientific/pi/portfolio-group/InterventionalOncology/therasphere/campaign/downloads/TheraSphere_dose_matters_brochure_PI-1165103-AB.pdf.

[28] Chang TT, Bourgeois AC, Balius AM, Pasciak AS. Treatment modification of yttrium-90 radioembolization based on quantitative positron emission tomography/CT imaging. J Vasc Interv Radiol 2013 Mar;24(3):333–7.
[29] Gulec SA, Sztejnberg ML, Siegel JA, Jevremovic T, Stabin M. Hepatic structural dosimetry in (90)Y microsphere treatment: a Monte Carlo modeling approach based on lobular microanatomy. J Nucl Med 2010 Feb;51(2):301–10.
[30] Kulkarni NM, Fung A, Kambadakone AR, Yeh BM. Computed Tomography Techniques, Protocols, Advancements, and Future Directions in Liver Diseases. Magn Reson Imaging Clin N Am 2021 Aug;29(3):305–20.
[31] Thirion JP. Image matching as a diffusion process: an analogy with Maxwell's demons. Med Image Anal 1998 Sep;2(3):243–60.
[32] Vercauteren T, Pennec X, Perchant A, Ayache N. Diffeomorphic demons: efficient non-parametric image registration. Neuroimage 2009 Mar;45(1 Suppl):S61–72.
[33] Russell Jr JL, Carden JL, Herron HL. Dosimetry calculations for yttrium-90 used in the treatment of liver cancer. Endocurietherapy/Hyperthermia. Oncology 1988;4:171–86.
[34] Hashikin N.A.A, Yeong C.H., Guatelli S., Abdullah B.J.J., Ng K.H., Malaroda A, et al. Organ doses from hepatic radioembolization with ^{90}Y, ^{153}Sm, ^{166}Ho and ^{177}Lu: A Monte Carlo simulation study using Geant^{4} J. Phys.: Conf. Ser. 694 012059, 2016.
[35] Sarrut D, Bała M, Bardiès M, et al. Advanced Monte Carlo simulations of emission tomography imaging systems with GATE. Phys Med Biol 2021. May 14;66(10.